

# Lithium-ion battery state-of-charge estimation based on deconstructed equivalent circuit at different open-circuit voltage relaxation times<sup>\*</sup>

Xi-ming CHENG<sup>†1</sup>, Li-guang YAO<sup>1</sup>, Michael PECHT<sup>2</sup>

(<sup>1</sup>Collaborative Innovation Center for Electric Vehicles in Beijing, National Engineering Laboratory for Electric Vehicles, Department of Vehicular Engineering, Beijing Institute of Technology, Beijing 100081, China)

(<sup>2</sup>Center of Advanced Life Cycle Engineering, University of Maryland, College Park, MD 20742, USA)

<sup>†</sup>E-mail: cxm2004@bit.edu.cn

Received Mar. 16, 2016; Revision accepted Oct. 12, 2016; Crosschecked Mar. 9, 2017

**Abstract:** Equivalent circuit model-based state-of-charge (SOC) estimation has been widely studied for power lithium-ion batteries. An appropriate relaxation period to measure the open-circuit voltage (OCV) should be investigated to both ensure good SOC estimation accuracy and improve OCV test efficiency. Based on a battery circuit model, an SOC estimator in the combination of recursive least squares (RLS) and the extended Kalman filter is used to mitigate the error voltage between the measurement and real values of the battery OCV. To reduce the iterative computation complexity, a two-stage RLS approach is developed to identify the model parameters, the battery circuit of which is divided into two simple circuits. Then, the measurement values of the OCV at varying relaxation periods and three temperatures are sampled to establish the relationships between SOC and OCV for the developed SOC estimator. Lastly, dynamic stress test and federal test procedure drive cycles are used to validate the model-based SOC estimation method. Results show that the relationships between SOC and OCV at a short relaxation time, such as 5 min, can also drive the SOC estimator to produce a good performance.

**Key words:** Lithium-ion batteries; Open-circuit voltage (OCV); State-of-charge (SOC); Recursive least squares (RLS); Extended Kalman filter (EKF)

<http://dx.doi.org/10.1631/jzus.A1600251>


**CLC number:** TM912.1

## 1 Introduction

Promising applications such as electric vehicles and smart grids have encouraged many researchers to improve lithium-ion (Li-ion) battery performance (Speirs *et al.*, 2014). One area of research is battery state estimation, especially the estimation of the state-of-charge (SOC). The SOC is used as a ruler to quantize a battery's capacity, power, energy, and thermal behavior.

There are three types of battery SOC estimation methods. The first method is ampere-hour (Ah) integration, and the second is open-circuit voltage (OCV) measurement. Although the Ah method is simple and reliable over a short period, it is easily disturbed by electromagnetic noises and thus can generate accumulative errors over a long period for the SOC calculation (Huria *et al.*, 2014). Due to the fact that the SOC is a function of the OCV, the OCV method is used to correct the Ah accumulative errors through the comparison between measurements and references of the battery OCV. Hence, both the Ah and OCV methods are combined to estimate the battery SOC (Waag *et al.*, 2014). However, the OCV values are affected by relaxation periods (Petzl and Danzer, 2013).

<sup>\*</sup> Project supported by the National Natural Science Foundation of China (No. 51677006)

 ORCID: Xi-ming CHENG, <http://orcid.org/0000-0001-5933-2630>  
 © Zhejiang University and Springer-Verlag Berlin Heidelberg 2017

The third method is model-based SOC estimation, which can combine the Ah integration and OCV methods in accurate battery models to correct battery SOC. In general, battery models include the equivalent circuit model and the electrochemical model. Due to heavy-load computation and difficult parameter identification, the electrochemical model should be either significantly order-reduced or reformulated for SOC estimation of built-in battery management systems (Northrop *et al.*, 2014). However, battery circuit models consist of simple resistance-capacitance (RC) components and perform well in real time for SOC estimation (Dai *et al.*, 2013; Seaman *et al.*, 2014).

Piller *et al.* (2001) first used the Kalman filter to estimate the battery SOC with simulated data on a hybrid electric vehicle. Plett (2004) presented an adaptive filter to estimate the Li-ion battery SOC based on circuit models. Since then, Kalman filtering technologies have been studied to provide solutions to nonlinear behaviors of batteries for circuit model-based SOC estimation, including unscented transform (Plett, 2006; Aung *et al.*, 2015), adaptive approaches (Wang *et al.*, 2009; Sun *et al.*, 2011; Xia *et al.*, 2015), and dual filtering (Mastali *et al.*, 2013; Xiong *et al.*, 2013b). Except for the above advanced filters, several topics have been discussed in the following contexts: adaption to variable operating conditions such as temperature, C-rates, and degradation (Dai *et al.*, 2013; Xiong *et al.*, 2013a; Xing *et al.*, 2014); correction of the SOC-OCV relationship for hysteresis voltage and flat plateau voltage for LiFePO<sub>4</sub> batteries (Huria *et al.*, 2014); denoised voltage measurements (Lee and Kim, 2015); different cells in series (Sepasi *et al.*, 2014).

Since the OCV is a controllable voltage source of the battery circuit model, the relaxation periods for OCV measurements have effects on model-based SOC estimation. Although long relaxation periods produce accurate OCV values for reliable SOC estimation, they are quite time-consuming for OCV measurements (Pei *et al.*, 2014). An appropriate relaxation period should be explored to ensure the accuracy of the circuit model-based SOC estimation for a short SOC-OCV test time. However, there is little literature discussing this.

We aim to investigate the accuracy of the circuit model-based SOC estimation driven by the relationships between SOC and OCV with different re-

laxation periods for a short SOC-OCV test time. The SOC-estimation algorithm is developed on the extended Kalman filter (EKF), the model parameters of which are identified online by the circuit deconstruction technique and the two-stage recursive least squares (RLS) method.

## 2 Combined estimation for model parameters and states

The second-order RC circuit as shown in Fig. 1 is commonly used to model Li-ion batteries because this battery equivalent circuit has better voltage approximation than the first-order RC circuit, and has less modeling complexity than the high-order RC circuits (Einhorn *et al.*, 2013). In Fig. 1, the controllable voltage source is the OCV. The internal resistor,  $R_0$ , indicates the resistance of electrons and ions moving in the electrodes and electrolyte, and  $R_1$ ,  $R_2$ ,  $C_1$ , and  $C_2$  represent the polarization effects of the battery cell.

Assuming that the working current is positive when the battery is charged, and vice versa, the SOC can be given as

$$s(t) = s(t_0) + \int_{t_0}^t [k_c i(\tau) / C_s] d\tau, \quad (1)$$

where  $s$  denotes the battery SOC,  $i$  the charging or discharging current,  $t_0$  the start time to re-compute the SOC,  $C_s$  the scaled nominal capacity, and  $k_c$  the coulombic efficiency which is defined as the ratio of the charge delivered by a rechargeable battery during the discharge cycle to the charge stored during the charge cycle (Khan *et al.*, 2014).

The second-order RC circuit can be expressed in the following equations:

$$\begin{cases} \dot{u}_1 = (-u_1 + R_1 i) / \tau_1, \\ \dot{u}_2 = (-u_2 + R_2 i) / \tau_2, \\ u_t = u_{OCV} + R_0 i + u_1 + u_2, \\ u_{re} = u_t - u_{OCV}, \\ u_{OCV} = f(s, T), \end{cases} \quad (2)$$

where  $u_{OCV}$  denotes the battery OCV,  $u_t$  the terminal voltage of the battery,  $\tau_1$  the time constant equaling

to  $R_1C_1$ ,  $\tau_2$  the time constant equaling to  $R_2C_2$ , and  $T$  the operating temperature.

When a battery is interrupted from being either charged or discharged, its terminal voltage changes in the relaxation periods even if the battery current is zero. The measurement values of OCV are affected by the relaxation periods and are only close to their real values at any SOC point. Hence, the OCV can be expressed as the sum of a measurement value and an error voltage:

$$u_{OCV} = u_{OCV,m} + e_{OCV}, \quad (3)$$

where  $u_{OCV,m}$  denotes the measurements of the battery OCV and  $e_{OCV}$  the errors between  $u_{OCV,m}$  and  $u_{OCV}$ .

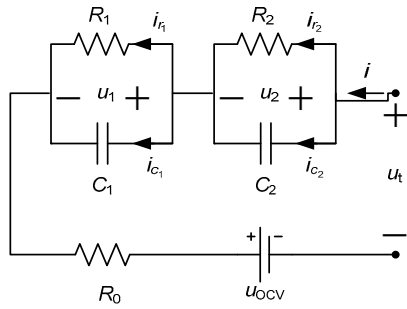


Fig. 1 Second-order RC circuit of the Li-ion battery

The parameters in Eq. (2) need to be extracted for battery modeling. Because the model parameters change with SOC, temperature, C-rate, and degradation, look-up tables and online-parameter estimators can be employed for an accurate battery voltage approximation under varying operation conditions (Hu et al., 2011; Ecker et al., 2012; Einhorn et al., 2013). The online estimators such as the RLS and Kalman filters can make the model parameters adaptive to working conditions without being rescaled for battery degradation like the look-up tables. Compared to the EKF, the RLS involves lower operational cost (Waag et al., 2014) and no dependency on noise covariance (Sayed, 2008) for model-parameter identification.

Before the RLS is used to identify parameters of the battery circuit model, the relationships between the OCV and SOC are known in advance because they have been validated in a wide SOC range for a decaying battery when the SOC is normalized

to its real capacities (Roscher et al., 2011; Ecker et al., 2012). However, there is no way for any numerical optimizer to separate parameters of the two RC branches in Fig. 1 and mitigate the fact that if the algorithm swaps parameters of the two RC branches, the simulation would not change (Jackey et al., 2013). Nevertheless, the estimated parameters of the battery circuit model can be negative by the RLS method (Cheng et al., 2016). Hence, a circuit deconstruction technique and two RLSs in series can be developed to online estimate parameters of the second-order RC circuit in Fig. 1. This circuit can be deconstructed into a first-order RC circuit and a single RC circuit (Fig. 2).

For the deconstructed circuits in Fig. 2, two RLSs are required to estimate the circuit parameters. The first RLS is used to estimate  $R_0$ ,  $R_1$ , and  $C_1$ . Then the second RLS is applied to estimate  $R_2$  and  $C_2$  by the battery voltage error sequence between the measurements and estimated values of the first-order RC circuit. The method stated above wherein the two RLSs are operated in series is named the two-stage RLS method, and its mathematical equations are described as follows.

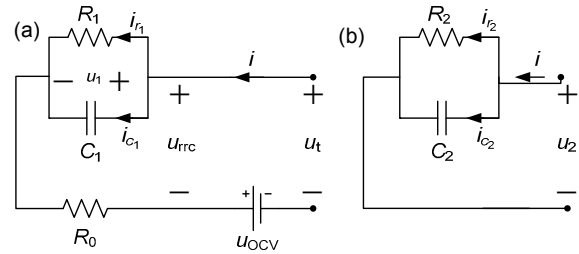


Fig. 2 Deconstructed circuits  
(a) First-order RC circuit; (b) Single RC circuit

By the transfer function and Euler integration method for the battery circuit in Fig. 2a (Fleischer et al., 2014; Cheng et al., 2016), the difference equation can be given as

$$u_{rrc,k} = b_0 i_k + b_1 i_{k-1} - a_1 u_{rrc,k-1}, \quad (4)$$

where  $b_0 = R_0$ ,  $b_1 = R_0(T_s/\tau_1 - 1) + R_1 T_s/\tau_1$ , and  $a_1 = T_s/\tau_1 - 1$ . Eq. (4) is transformed to the following form:

$$y_{1,k} = \mathbf{h}_{1,k}^T \boldsymbol{\theta}_1 + e_{1,k}, \quad (5)$$

where  $e_{1,k}$  denotes the discrete value at time  $k$  of the white noise sequence,  $y_{1,k}=u_{rc,k}$ ,  $\theta_1=[b_0 \ b_1 \ a_1]^T$ , and  $h_{1,k}^T=[i_k \ i_{k-1} - u_{rc,k-1}]$ .

From Eqs. (2), (3), and (5), it can be seen that the estimated parameters in  $\theta_1$  can be influenced by the error voltage  $e_{OCV}$ . There is no similar tendency for how the model parameters evolve with a relaxation period at 10 min, 30 min, 1 h, 6 h, or 12 h (Leng et al., 2014).

At every turn, the RLS method is used to estimate model parameters of the first-order RC circuit in Fig. 2a. By Eq. (5), the estimated equation is

$$y_{1,k}^* = h_{1,k}^T \theta_1^*, \quad (6)$$

where  $y_{1,k}^*$  denotes the estimated battery voltage and  $\theta_1^*$  the vector of the estimated parameters.

Then the error-voltage equation can be given:

$$\Delta u_{1,k} = u_{rc,k} - y_{1,k}^*, \quad (7)$$

where  $\Delta u_{1,k}$  is the estimation error of the battery voltage.

Then  $\Delta u_{1,k}$  is compensated by the single RC circuit. Similarly, its difference equation can be written as

$$y_{2,k} = h_{2,k}^T \theta_2 + e_{2,k}, \quad (8)$$

where  $e_{2,k}$  represents the discrete value at time  $k$  of the white noise sequence,  $y_{2,k}=\Delta u_{1,k}$ ,  $\theta_2=[d_1 \ c_1]^T$ , and  $h_{2,k}^T=[i_{k-1} - y_{2,k-1}]$ .

Therefore, the parameters of the single RC circuit can be calculated as follows:

$$\begin{cases} \tau_2 = T_s / (1 + c_1), \\ R_2 = d_1 / T_s. \end{cases} \quad (9)$$

For the two-state RLS algorithm stated above, there are  $3 \times 3$  matrix operations in the first RLS for  $\theta_1$ , and  $2 \times 2$  matrix operations in the second RLS for  $\theta_2$  in every iterative operation. Compared to the five-parameter estimator for Fig. 1, the three-parameter estimator for Fig. 2a and two-parameter estimator for Fig. 2b make the computation simpler.

After building the two-stage RLS algorithm for model-parameter estimation, the EKF is used to estimate model states including the battery SOC (Lee et al., 2007). The discrete equations of state estimation can also be given as

$$\begin{cases} X_{k+1} = \Phi_k X_k + G_k i_{k+1} + \omega_k, \\ u_{t,k} = F_k(X_k) + D i_k + v_k, \end{cases} \quad (10)$$

where system states, coefficient matrices, and variables can be expressed respectively as

$$\begin{aligned} X &= [s \ u_{1,t} \ u_{2,t}]^T, \\ \Phi_k &= \begin{bmatrix} 1 & 0 & 0 \\ 0 & e^{-T_s/\tau_1} & 0 \\ 0 & 0 & e^{-T_s/\tau_2} \end{bmatrix}, \\ G_k &= [k_c T_s \ R_1(1 - e^{-T_s/\tau_1}) \ R_2(1 - e^{-T_s/\tau_2})]^T, \\ F_k(X_k) &= u_{OCV,k} + u_{1,k} + u_{2,k}, \\ D &= R_0. \end{aligned}$$

Because the observation equation in Eq. (10) is a nonlinear function of the state vector, the observation matrix  $H_k$  can be given as

$$H_k = [\partial F / \partial X]_k. \quad (11)$$

When the model parameters, process and observation noises are given in Eq. (10), the battery SOC can be deduced from the EKF (Plett, 2004).

The model parameters in Eq. (2) evolve with operational conditions to affect the model accuracy, so that the EKF-based SOC estimator should run with the parameter identifier of the two-stage RLS approach. The combined algorithm is stated in Fig. 3, the flowchart of which is similar to that of the dual Kalman filter (Haykin, 2001).

In Fig. 3, the adaptive algorithm needs to be initialized for two RLSs and one EKF. The former initialization includes three resistances, two capacitances, and two covariance matrices  $\theta_{1,0}$  and  $\theta_{2,0}$ . The latter is initialized by three states in Eq. (10) and three covariances  $P_0$ ,  $Q_k$ , and  $R_k$ . After initialization, the combined parameter identification and state estimation algorithm runs in a closed loop. Driven by the battery current and terminal voltage, the two-stage

RLS approach identifies and outputs the five model parameters to the EKF-based SOC estimator. Then the SOC estimator runs to produce the estimated SOC for the parameter identifier.

### 3 Experimental setup

Three CBAK 2.0 Ah 18650 power Li-ion cells in series were placed in a temperature chamber and discharged/charged by a Digatron battery tester BNT 100-60-ME for this experiment. The specification of the power Li-ion battery is shown in Table 1. There are three types of battery charged/discharged tests: capacity, OCV, and drive cycle tests. The battery charging or discharging capacities were limited up to the nominal value in the OCV and drive cycle tests.

#### 1. Capacity test

The battery cells were placed in a chamber at 20 °C. In a charging-discharging round, cells were first charged at 0.5C constant current (CC) up to the maximum voltage, and immediately switched at the constant voltage (CV) charge for 1 h. Then they

were discharged at 1.0C constant discharging current (DC) down to the minimum voltage, and then discharged at 0.2C DC down to the same cutoff voltage. There were three identical rounds for the battery capacity test, by which the battery nominal capacity was confirmed in Table 1.

Coulombic efficiency test: the battery cells were placed in a chamber at 0, 20, and 40 °C, respectively. At each operational temperature, these cells were charged in a CC-CV mode with the same up-limited voltage for the nominal capacity. After a 2-h battery rest, cells were discharged in a CC mode down to the cutoff voltage for a discharging capacity. Parameter  $k_c$  in Eq. (1) was equal to 0.897 at 0 °C, 0.993 at 20 °C, or 0.999 at 40 °C, respectively.

#### 2. OCV test

During the charging OCV test, cells were rested for 2 h after every 10% nominal capacity pulse charge at 0.5C above 10 °C or 0.2C below 10 °C. After they were fully charged and rested for 2 h, they were discharged at 20 °C, the discharging procedure of which was the same as that of the capacity test. After the cells were empty, they were

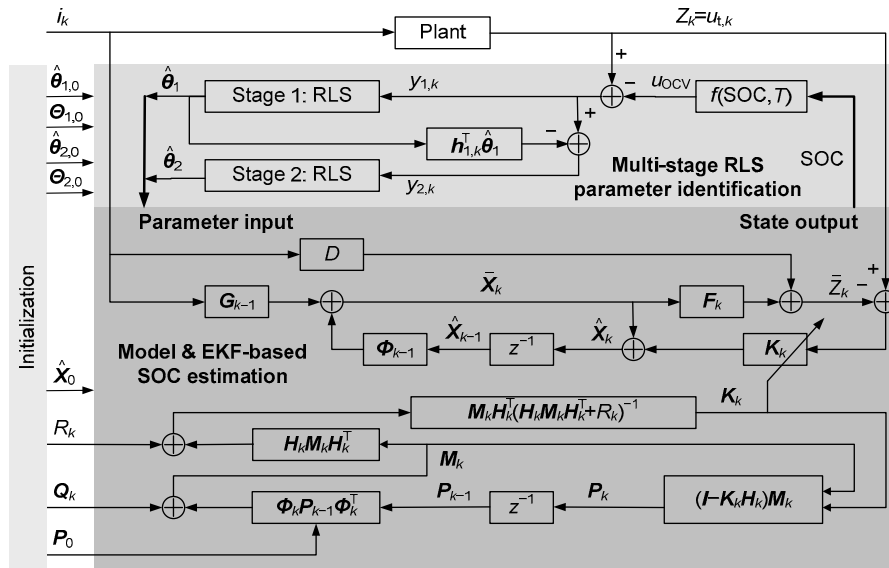


Fig. 3 Block diagram of the two-stage RLS-EKF SOC estimation algorithm.  $\theta_{1,0}$  and  $\theta_{2,0}$  are for the two-stage RLS initialization, while  $P_0$ ,  $Q_k$ , and  $R_k$  are for the EKF algorithm initialization

Table 1 Specification of the Li-ion cell

Nominal capacity (Ah)	Voltage (V)			Maximum C-rate (C)		Temperature (°C)	
	Minimum	Nominal	Maximum	Charge	Discharge	Charge	Discharge
2.0	2.75	3.7	4.2	1.0	2.0	0–45	–20–60

charged at 20 °C, the charging procedure of which was the same as that of the capacity test. Furthermore, they were rested for 2 h after every 10% nominal capacity pulse discharge at 0.5C at 0, 20, and 40 °C respectively, the cutoff voltage of which was checked. If the first discharging cutoff voltage occurred, they would be continuously discharged at 0.2C down to the cutoff voltage.

### 3. Drive cycle test

Both the dynamic stress test (DST) and federal test procedure (FTP) were conducted to test these cells. During the battery tests, their overvoltage was limited up to the maximum voltage, which could happen at the initial regenerative current pulses, especially under low temperatures.

## 4 Results

The performance of the OCV-based SOC estimation was first evaluated from the experimental data for comparison with that of the model-based SOC estimation. Then the two-stage RLS approach was demonstrated by an example. Finally, the combined algorithm for SOC estimation was developed, the performance of which would be discussed under the relationships between SOC and OCV at varying relaxation periods and temperatures. Note that in the figures, 'CHA' represents the battery charging process while 'DCH' represents the battery discharging process.

### 4.1 Influence of varying relaxation periods on OCV-based SOC estimation

The measurement values of 2-h OCV are illustrated in Fig. 4, the entropy values of which rise on average by 0.99 mV/°C from 20 °C to 0 °C and by 0.45 mV/°C from 40 °C to 20 °C for charging. As the battery discharges, the entropy values drop on average by 0.44 mV/°C from 20 °C to 0 °C and by -0.15 mV/°C from 40 °C to 20 °C.

Compared to the 2-h OCV, the relative error of OCV measurements at different relaxation periods is defined as follows:

$$r_e = 100\% \times (y_t - y_{2h}) / y_{2h}, \quad (12)$$

where  $y_t$  denotes the OCV measurements at different

relaxation periods and  $y_{2h}$  the measurement value at the 2-h relaxation period.

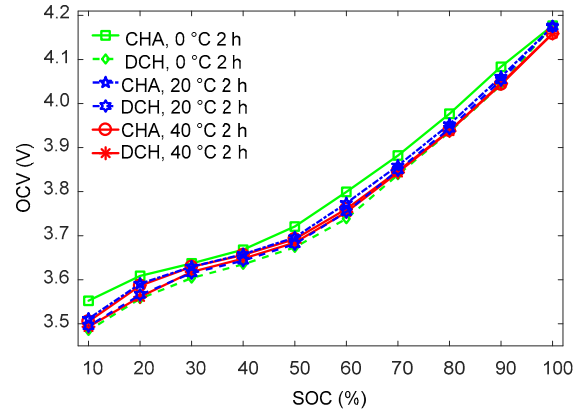


Fig. 4 Battery SOC-OCV curves

The relative errors at 0, 20, and 40 °C are shown in Figs. 5–7 (at 5, 10, 30, and 60 min), respectively. Several behaviors can be observed. The SOC-OCV relative error curves at the same intervals are not monotonic, regardless of whether the battery is charged or discharged at different temperatures. The OCV relative errors are less than 1%, except for the 5-min values of the relaxation process after charging the battery at 0 °C.

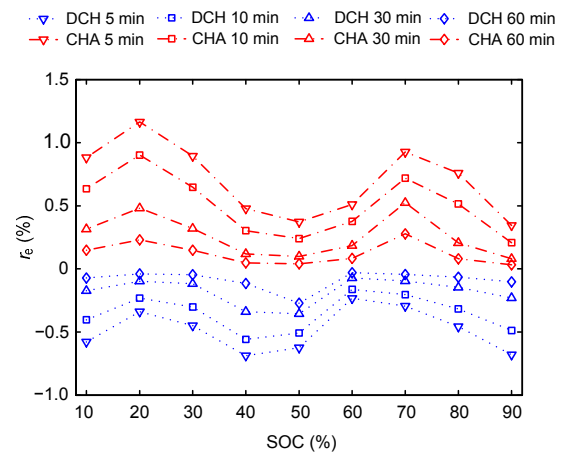


Fig. 5 Battery OCV error curves at 0 °C

The average slope of the SOC-OCV curves is used as the baseline for the OCV-based estimation method, which is 0.6864 V/SOC between 10% SOC and 90% SOC in Fig. 4. The absolute maximum value of all discharging OCV errors is up to 0.0278 V at 5 min and 0 °C, the SOC error of which is about

4.1%. At the other relaxation intervals, the corresponding SOC error is less than 3% at 10 min, 2% at 30 min, or 1.5% at 60 min, respectively. However, the charging OCV error can reach 0.0419 V at 5 min and 0 °C, causing about a 6.1 % SOC error. Similarly, the corresponding charging SOC error at 0 °C is less than 4.7% at 10 min, 3% at 30 min, or 1.6 % at 60 min, respectively.

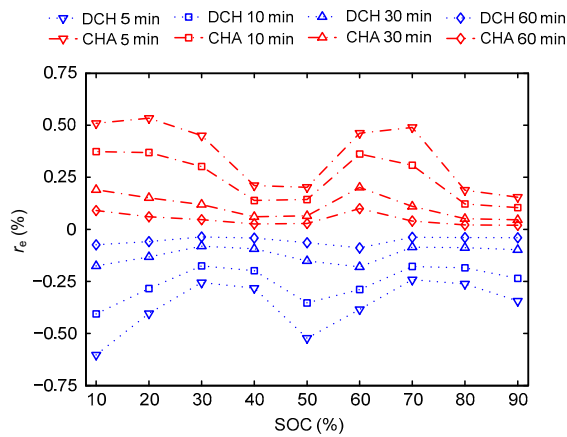


Fig. 6 Battery OCV error curves at 20 °C

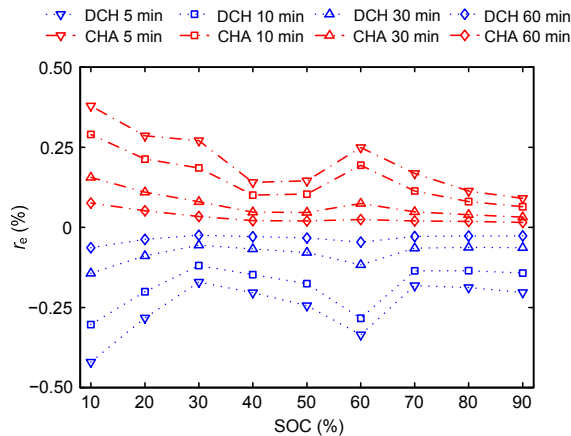


Fig. 7 Battery OCV error curves at 40 °C

## 4.2 Validation of the two-stage RLS approach

The Li-ion battery is excited by the DST current at 20 °C (Fig. 8a). The SOC decreases from 100% to 10% (Fig. 8b). This test signal includes four stages represented in SOC ranges, i.e., stage A (100%, 87%), stage B (87%, 46%), stage C (46%, 12%), and stage D (12%, 10%). In zone A, the excitation current is limited to avoid overvoltage of the full battery.

Owing to the large plot scale, it is difficult to discriminate among the voltage curves in Fig. 8c, the voltage differences of which can be enlarged on a small scale. The battery terminal voltage errors between the real and model values are drawn in Fig. 8d. The root mean square (RMS) is 2.8 mV for the first-order RC circuit model and 2.1 mV for the deconstructed second-order RC circuit model. By the developed two-stage RLS approach applied for the deconstructed second-order RC circuit model driven by the DST, the RMS voltage error drops by 25% compared to the first-order RC circuit model.

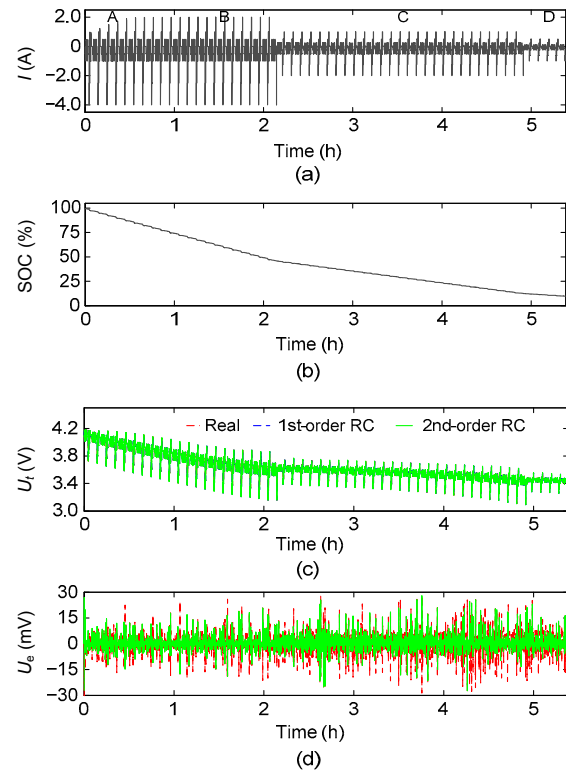


Fig. 8 Battery DST profiles and identification results at 20 °C

(a) Current; (b) SOC; (c) Battery voltage; (d) Voltage errors

The online parameter identifiers ran on MATLAB in a laptop running Win7 and with an Intel i5-3210M CPU @ 2.50 GHz. For the total running time of parameter identifiers, the RLS almost ran for the same period, about 0.9516 s, for the first- and second-order RC circuit models. Compared to the RLS, the two-stage RLS approach spent about 1.3104 s on identifying battery parameters of the second-order RC circuit model even though it has

less complexity. However, the parameters of one of the RC branches of the second-order RC circuit can be identified as negative by the RLS (Cheng *et al.*, 2016).

Associated with Fig. 8, the results of the identified parameters are shown in Fig. 9. The online identified parameters  $R_0$ ,  $R_1$ ,  $\tau_1$ , and  $R_2$  have the tendency to increase when the battery SOC decreases. The single RC circuit in Fig. 2b was used as a proportion-integration regulator to compensate for the model voltage errors resulting from the first-order RC circuit in Fig. 2a, the spikes of which could cause  $R_2$  and  $\tau_2$  to fluctuate with a large amplitude. A moving average filter was applied to obtain a smooth  $\tau_2$  and reduce the model voltage errors.

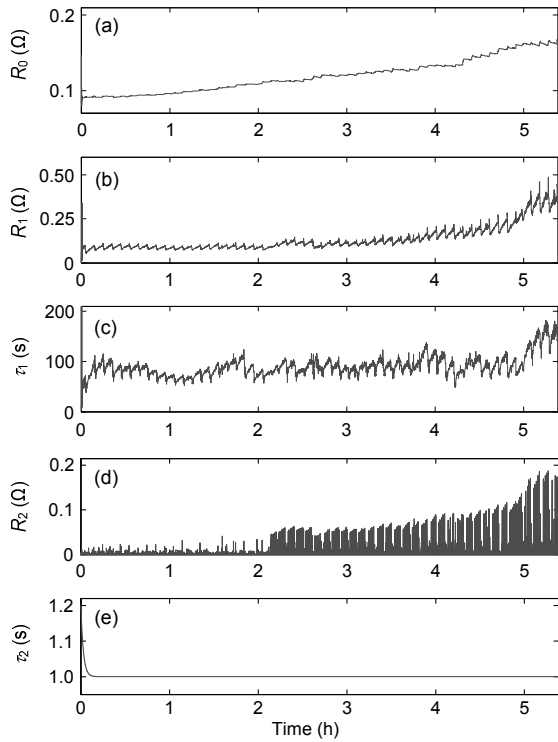


**Fig. 9** Parameters of Fig. 2 identified online for battery DST profile at 20 °C: (a)  $R_0$ ; (b)  $R_1$ ; (c)  $\tau_1$ ; (d)  $R_2$ ; (e)  $\tau_2$

#### 4.3 Influence of varying relaxation periods on model-based SOC estimation

The battery SOC was estimated by the combined algorithm in Fig. 3 driven by the relationships between SOC and OCV at varying relaxation periods and temperatures.

In this adaptive algorithm, the two-stage RLS had the same initialization as the DST in Section 4.2. The EKF-based SOC estimator should also be initialized. Because the Kalman gain  $K_k$  and covariance matrix  $P_k$  are directly associated with the noise covariance matrix  $Q_k$  and scalar  $R_k$  in Fig. 3, the optimality of the EKF performance depends on their initial values. Theoretically, the two noises are assumed zero-mean Gaussian distributions and uncorrelated, and are computed from the process and observation of a plant. The filter uses the battery dynamic lagging error information to reconstruct covariance matrices instead of constants, namely, an adaptive Kalman filter (AKF). However, the AKF not only has not yet been strictly proven in optimal theories, but also aggravates the computation burden of Kalman filter (Chui and Chen, 2009). In practice, due to the limited knowledge of internal states and real-time disturbances of batteries, both  $Q_k$  and  $R_k$  were normally adopted by trial and error (Khan *et al.*, 2014). The initial values of the EKF are given as follows:

$$\begin{aligned} Q_0 &= \begin{bmatrix} 10^{-6} & 0 & 0 \\ 0 & 10^{-6} & 0 \\ 0 & 0 & 10^{-6} \end{bmatrix}, \\ P_0 &= \begin{bmatrix} 0.01 & 0 & 0 \\ 0 & 1.0 & 0 \\ 0 & 0 & 1.0 \end{bmatrix}, \\ X_0 &= [1.0 \quad 0.0 \quad 0.0]^T, \text{ and } R_0 = 100.00. \end{aligned} \quad (13)$$

The combined algorithm was driven by the FTP signal, one of which is shown in Fig. 10. Three FTP drive cycles had different average values of  $-0.26$  A at 0 °C,  $-0.3$  A at 20 °C, and  $-0.33$  A at 40 °C, respectively. The voltage error in the RMS is 9.8 mV as shown by the 2-h SOC-OCV curves in Fig. 10c; the value was much larger than that of the DST in Fig. 8d. This is because this profile makes the tested battery more dynamic in current and voltage than the DST. The curves of identified parameters by the combined algorithm are similar to those of the DST in Fig. 9.

Associated with Fig. 10, the SOC estimation and error curves are shown in Fig. 11. It is difficult to discriminate between the estimation and real



values of battery SOC in Fig. 11a. At 20 °C, the SOC errors are used to compare their influences with the relationships between SOC and OCV at different relaxation periods in Fig. 11b. If the model is accurate, the value of  $R_k$  should be chosen based on the accuracy of the voltage sensor used in the experiments. For a significantly nonlinear battery system,  $R_k$  can be affected by errors resulting from the model simplification, parameter variations, linearization, and discretization. For example, the observation noises could be colored through Eqs. (3) and (10). Hence, by the adjustable level of observation noise, the EKF becomes robust to the model errors (Lee *et al.*, 2007). The value of  $R_k$  can be adjustable between zero and infinity for a good estimation. In this adaptive algorithm, the low initial value of  $R_k$  can make the EKF tract fast.  $R_k$  is set at 20 times its initial value after the filter startup to reduce SOC estimation errors.

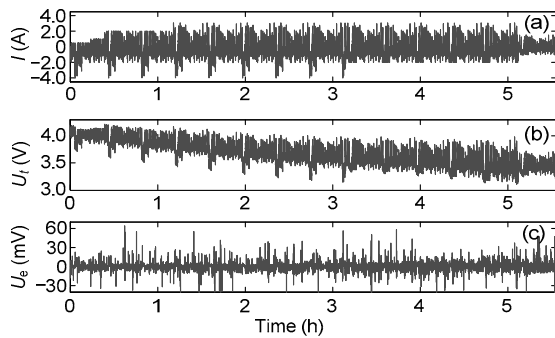


**Fig. 10** Battery FTP profiles and terminal voltage errors at 20 °C

(a) Excitation current; (b) Voltage measurements; (c) Voltage estimation errors

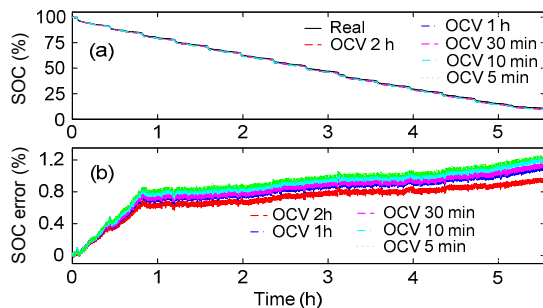


**Fig. 11** Estimated SOC and errors impacted by different measurement time instantaneous OCVs for battery FTP profiles at 20 °C

(a) Real and estimated SOC curves; (b) SOC estimation errors

The absolute maximum value of their SOC estimation errors is 1.07% for the 2-h SOC-OCV curves. Compared to the maximum SOC estimation errors for the 2-h SOC-OCV curve, those for the 1 h, 30 min, 10 min, and 5 min curves can increase by 4.42%, 7.41%, 13.9%, and 15%, respectively.

The battery SOC estimation is also affected by the working temperature (Figs. 12 and 13). The SOC estimation errors at 0 °C in Fig. 12b are 2.44% for the 2-h SOC-OCV relationship, and 2.61% for the 5-min curve. Similarly, the SOC estimation errors at 40 °C in Fig. 13b are 0.96% for the 2-h SOC-OCV relationship, and 1.07% for the 5-min curve. Compared to the OCV estimation values at 20 °C, the FTP at 0 °C shows an SOC estimation error increase by 1.37%, and this drive cycle at 40 °C drops by 0.09%.

In addition, the OCV values at 20 °C are used to estimate the SOC at both 0 °C and 40 °C. There is a small gap of about 0.12% between the two SOC error curves at the end of the working period in Fig. 12b. However, the two SOC error curves have

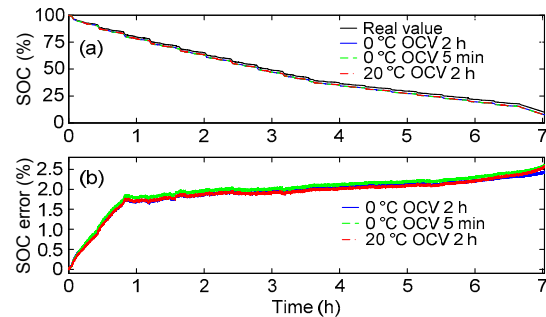


**Fig. 12** Estimated SOC and errors impacted by different temperature OCVs for battery FTP profiles at 0 °C

(a) Real and estimated SOC curves; (b) SOC estimation errors

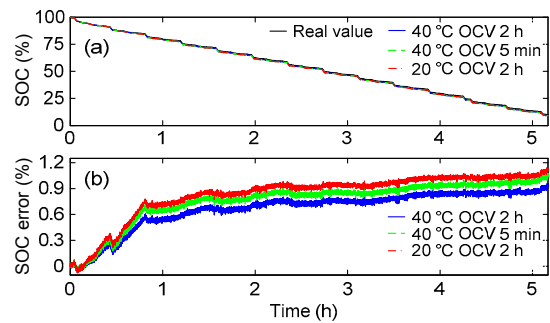


**Fig. 13** Estimated SOC and errors impacted by different temperature OCVs for battery FTP profiles at 40 °C

(a) Real and estimated SOC curves; (b) SOC estimation errors

an obvious gap by a small amount in Fig. 13b, which is about 0.19%.

## 5 Conclusions

On the basis of the deconstructed circuit, we combined a two-stage RLS and EKF to estimate both model parameters and battery SOC. For this methodology and the OCV-based method, the relationships between SOC and OCV at varying relaxation periods and temperatures were investigated for the Li-ion battery SOC estimation.

Compared to the 2-h OCV, the absolute maximum value of the OCV relative errors was smaller at higher temperatures. Using the OCV-based SOC estimation method, different relaxation times were required to obtain SOC estimation errors less than 5% at 0 °C, 5 min for the discharging process, and 10 min for the charging process.

The deconstructed circuit and two-stage RLS approach were integrated to identify parameters of the second-order RC circuit online. This approach reduced the battery voltage estimation error by 25% compared to the first-order RC circuit.

The developed adaptive algorithm showed that the SOC estimation accuracy improves as the OCV relaxation periods increase and that the SOC estimation errors can be reduced. Based on the SOC-OCV relationship at 5-min relaxation time and 0 °C, the model-based estimator yields a 2.61% SOC estimation error and decreases by 1.49% compared to the OCV-based method. Moreover, the SOC-OCV relationship at room temperature was used to estimate the SOC at different temperatures, which generated a minimum SOC estimation error of less than 0.2%. With this OCV analysis and SOC estimation methods, not only was the SOC estimation accuracy improved, but also the OCV test time is reduced down to a 5-min relaxation period for the SOC-OCV relationships. In future work, the reliable SOC estimation of LiFePO<sub>4</sub> batteries at different relaxation voltage measurement intervals will be studied.

## References

- Aung, H., Low, K.S., Goh, S.T., 2015. State-of-charge estimation of lithium-ion battery using square root spherical unscented Kalman filter (Sqrt-UKFST) in nanosatellite. *IEEE Transactions on Power Electronics*, **30**(9):4774-4783.  
<http://dx.doi.org/10.1109/TPEL.2014.2361755>
- Cheng, X., Yao, L., Xing, Y., et al., 2016. Novel parametric circuit modeling for Li-ion batteries. *Energies*, **9**(7):539-553.  
<http://dx.doi.org/10.3390/en9070539>
- Chui, C.K., Chen, G., 2009. Kalman Filtering with Real-time Applications. Springer, Berlin, Germany, p.181-184.
- Dai, H., Zhang, X., Wei, X., et al., 2013. Cell-BMS validation with a hardware-in-the-loop simulation of lithium-ion battery cells for electric vehicles. *International Journal of Electrical Power and Energy Systems*, **52**:174-184.
- Ecker, M., Gerschler, J.B., Vogel, J., et al., 2012. Development of a lifetime prediction model for lithium-ion batteries based on extended accelerated aging test data. *Journal of Power Sources*, **215**:248-257.  
<http://dx.doi.org/10.1016/j.jpowsour.2012.05.012>
- Einhorn, M., Conte, F.V., Kral, C., et al., 2013. Comparison, selection, and parameterization of electrical battery models for automotive applications. *IEEE Transactions on Power Electronics*, **28**(3):1429-1437.  
<http://dx.doi.org/10.1109/TPEL.2012.2210564>
- Fleischer, C., Waag, W., Heyn, H.M., et al., 2014. On-line adaptive battery impedance parameter and state estimation considering physical principles in reduced order equivalent circuit battery models: Part 1. Requirements, critical review of methods and modeling. *Journal of Power Sources*, **260**:276-291.  
<http://dx.doi.org/10.1016/j.jpowsour.2014.01.129>
- Haykin, S., 2001. Kalman Filtering and Neural Networks. John & Wiley Inc., New York, USA, p.123-174.
- Hu, X., Sun, F., Cheng, X., 2011. Recursive calibration for a lithium iron phosphate battery for electric vehicles using extended Kalman filtering. *Journal of Zhejiang University-SCIENCE A (Applied Physics & Engineering)*, **12**(11):818-825.  
<http://dx.doi.org/10.1631/jzus.A1100141>
- Huria, T., Ludovici, G., Lutzemberger, G., 2014. State of charge estimation of high power lithium iron phosphate cells. *Journal of Power Sources*, **249**:92-102.  
<http://dx.doi.org/10.1016/j.jpowsour.2013.10.079>
- Jackey, R., Saginaw, M., Sanghvi, P., et al., 2013. Battery model parameter estimation using a layered technique: an example using a lithium iron phosphate cell. *SAE Technical Paper*, 2013-01-1547.  
<http://dx.doi.org/10.4271/2013-01-1547>
- Khan, M.R., Mulder, G., van Mierlo, J., 2014. An online framework for state of charge determination of battery systems using combined system identification approach. *Journal of Power Sources*, **246**:629-641.  
<http://dx.doi.org/10.1016/j.jpowsour.2013.07.092>
- Lee, J., Nam, O., Cho, B.H., 2007. Li-ion battery SOC estimation method based on the reduced order extended

- Kalman filtering. *Journal of Power Sources*, **174**(1):9-15. <http://dx.doi.org/10.1016/j.jpowsour.2007.03.072>
- Lee, S., Kim, J., 2015. Discrete wavelet transform-based denoising technique for advanced state-of-charge estimator of a lithium-ion battery in electric vehicles. *Energy*, **83**:462-473. <http://dx.doi.org/10.1016/j.energy.2015.02.046>
- Leng, F., Tan, C.M., Yazami, R., et al., 2014. A practical framework of electrical based online state-of-charge estimation of lithium ion batteries. *Journal of Power Sources*, **255**:423-430. <http://dx.doi.org/10.1016/j.jpowsour.2014.01.020>
- Mastali, M., Vazquez-Arenas, J., Fraser, R., et al., 2013. Battery state of the charge estimation using Kalman filtering. *Journal of Power Sources*, **239**:294-307. <http://dx.doi.org/10.1016/j.jpowsour.2013.03.131>
- Northrop, P.W.C., Suthar, B., Ramadesigan, V., et al., 2014. Efficient simulation and reformulation of lithium-ion battery models for enabling electric transportation. *Journal of the Electrochemical Society*, **161**(8):E3149-E3157. <http://dx.doi.org/10.1149/2.018408jes>
- Pei, L., Wang, T., Lu, R., et al., 2014. Development of a voltage relaxation model for rapid open-circuit voltage prediction in lithium-ion batteries. *Journal of Power Sources*, **253**:412-418. <http://dx.doi.org/10.1016/j.jpowsour.2013.12.083>
- Petzl, M., Danzer, M.A., 2013. Advancements in OCV measurement and analysis for lithium-ion batteries. *IEEE Transactions on Energy Conversion*, **28**(3):675-681. <http://dx.doi.org/10.1109/TEC.2013.2259490>
- Piller, S., Perrin, M., Jossen, A., 2001. Methods for state-of-charge determination and their applications. *Journal of Power Sources*, **96**(1):113-120. [http://dx.doi.org/10.1016/S0378-7753\(01\)00560-2](http://dx.doi.org/10.1016/S0378-7753(01)00560-2)
- Plett, G.L., 2004. Extended Kalman filtering for battery management systems of LiPB-based HEV battery packs: Part 3. State and parameter estimation. *Journal of Power Sources*, **134**(2):277-292. <http://dx.doi.org/10.1016/j.jpowsour.2004.02.033>
- Plett, G.L., 2006. Sigma-point Kalman filtering for battery management systems of LiPB-based HEV battery packs: Part 1. Introduction and state estimation. *Journal of Power Sources*, **161**(2):1356-1368. <http://dx.doi.org/10.1016/j.jpowsour.2006.06.003>
- Roscher, M.A., Assfalg, J., Bohlen, O.S., 2011. Detection of utilizable capacity deterioration in battery systems. *IEEE Transactions on Vehicle Technology*, **60**(1):98-103. <http://dx.doi.org/10.1109/TVT.2010.2090370>
- Sayed, A.H., 2008. Adaptive Filters. John Wiley & Sons, Inc., Hoboken, New Jersey, USA, p.501-508.
- Seaman, A., Dao, T.S., McPhee, J., 2014. A survey of mathematics-based equivalent-circuit and electrochemical battery models for hybrid and electric vehicle simulation. *Journal of Power Sources*, **256**:410-423. <http://dx.doi.org/10.1016/j.jpowsour.2014.01.057>
- Sepasi, S., Ghorbani, R., Liaw, B.Y., 2014. Improved extended Kalman filter for state of charge estimation of battery pack. *Journal of Power Sources*, **255**:368-376. <http://dx.doi.org/10.1016/j.jpowsour.2013.12.093>
- Speirs, J., Contestabile, M., Houari, Y., et al., 2014. The future of lithium availability for electric vehicle batteries. *Renewable and Sustainable Energy Reviews*, **35**:183-193. <http://dx.doi.org/10.1016/j.rser.2014.04.018>
- Sun, F., Hu, X., Zou, Y., et al., 2011. Adaptive unscented Kalman filtering for state of charge estimation of a lithium-ion battery for electric vehicles. *Energy*, **36**(5):3531-3540.
- Waag, W., Fleischer, C., Sauer, D.U., 2014. Critical review of the methods for monitoring of lithium-ion batteries in electric and hybrid vehicles. *Journal of Power Sources*, **258**:321-339. <http://dx.doi.org/10.1016/j.jpowsour.2014.02.064>
- Wang, J., Guo, J., Ding, L., 2009. An adaptive Kalman filtering based state of charge combined estimator for electric vehicle battery pack. *Energy Conversion and Management*, **50**(12):3182-3186. <http://dx.doi.org/10.1016/j.enconman.2009.08.015>
- Xia, B., Wang, H., Tian, Y., et al., 2015. State of charge estimation of lithium-ion batteries using an adaptive cubature Kalman filter. *Energies*, **8**(6):5916-5936. <http://dx.doi.org/10.3390/en8065916>
- Xing, Y., He, W., Pecht, M., et al., 2014. State of charge estimation of lithium-ion batteries using the open-circuit voltage at various ambient temperatures. *Applied Energy*, **113**:106-115. <http://dx.doi.org/10.1016/j.apenergy.2013.07.008>
- Xiong, R., Sun, F., Chen, Z., et al., 2013a. A data-driven multi-scale extended Kalman filtering based parameter and state estimation approach of lithium-ion polymer battery in electric vehicles. *Applied Energy*, **113**:463-476. <http://dx.doi.org/10.1016/j.apenergy.2013.07.061>
- Xiong, R., Sun, F., He, H., et al., 2013b. A data-driven adaptive state of charge and power capability joint estimator of lithium-ion polymer battery used in electric vehicles. *Energy*, **63**:295-308. <http://dx.doi.org/10.1016/j.energy.2013.10.027>

## 中文概要

**题目：**不同开路电压松弛时间下基于等效电路解构的锂离子电池荷电状态估计

**目的：**开路电压是基于模型的电池荷电状态估计的必要参数，其测试耗时大、效率低。本文旨在测试各种电压松弛时间的荷电状态-开路电压关系，研究其对开路电压法和等效电路模型的荷

电状态估计准确度的影响，提高开路电压测试效率。

**创新点：**1. 通过电路解构方法，将二阶阻容电路分解为简单路，运用二阶段递推最小二乘法辨识电路模型的参数；2. 基于递推最小二乘法和卡尔曼滤波算法，建立电路参数辨识和荷电状态估计的联合自适应算法，研究电池电压松弛时间对基于等效电路模型的荷电状态估计的影响。

**方法：**1. 通过电路解构技术和理论推导，构建辨识二阶阻容等效电路参数的二阶段递推最小二乘法辨识方法（图 2 和公式（4）~（9））；2. 将二阶段递推最小二乘法和扩展卡尔曼滤波器集成，建立适应工况变化的电池模型参数辨识和

状态估计的联合算法（图 3）；3. 通过电池测试，建立多温度和多电压松弛时间的荷电状态与开路电压的关系，驱动自适应联合算法，获得既保证荷电状态估计准确度，又缩短开路电压测试时间的电压松弛时间。

**结论：**1. 二阶段递推最小二乘法既能简化矩阵计算，又能够保证电路参数的辨识非负性；2. 联合自适应算法能够适应工况变化辨识模型参数和估计荷电状态；3. 联合自适应算法的结果表明，5 min 的电压松弛时间既能保证荷电状态估计性能，又能极大地提高开路电压测试效率。

**关键词：**锂离子电池；开路电压；荷电状态；递推最小二乘法；扩展卡尔曼滤波器